

Scalable Fluidic Matrix Circuits for Controlling Large Arrays of Individually Addressable Actuators

Saurabh Jadhav, Paul E. Glick, Michael Ishida, Christian Chan, Iman Adibnazari, Jurgen P. Schulze, Nick Gravish, and Michael T. Tolley*

A fundamental challenge of pneumatically powered soft robotic devices is the scalability of fluidic control systems to address each actuated degree of freedom, as the required electromechanical valves are bulky and expensive. Previous solutions have compromised the reprogrammability and/or the bandwidth of the fluidic system. This article describes and models a fluidic subsystem, a *fluidic matrix circuit (FMC)*, that enables the independent control of many (N^2) actuators using a limited number ($2N$) of electromechanical valves. The fundamental unit, a *fluidic logic module (FLM)*, generates a bidirectional pressure signal (vacuum or positive pressure) based on the state of the mass flow through it. Thus an array of pneumatic actuators can be addressed individually using an array of FLMs integrated into a matrix (i.e., an FMC), with electromechanical valves to switch the mass flow through each row and column of the matrix. The resulting refresh rates are an order of magnitude faster than previous approaches. This concept with a prototype FMC able to control 25 actuators using 10 electromechanical valves for applications including a fluidic shape display and a wearable haptic vest is demonstrated. This approach could enable more complex and sophisticated soft robotic devices with scalable control hardware.

1. Introduction

The physical intelligence embodied in soft robots and their ability to conform to complex topographies have made them attractive for applications ranging from robot navigation on unstructured terrain to exoskeletons for wearable haptics.^[1–5] Several approaches have been presented for the actuation of soft robotic devices, including fluidics (pneumatics and hydraulics), smart materials responsive to external stimuli, and tendons driven by electric motors.^[3,5,6] Among these actuation methods, pneumatic actuation has proven to be the most popular due to the commercial availability of control components (electromechanical valves and pumps), ease of power delivery, high system bandwidth, robust fabrication methods, and the existence of lightweight actuators.^[6–9] Furthermore, pneumatics offer versatility in modes of actuation, providing both positive pressure to inflate or pressurize bladders^[10] and vacuum to achieve variable

stiffness,^[11–13] which present a multitude of opportunities for controlling soft robots.


However, a significant challenge in pneumatic actuation is the scalability of fluidic control systems.^[3,6,9] The sophistication and complexity of many soft robots critically rely on the simultaneous and independent control of multiple actuators.^[6,9,14] While it is possible for multiple actuators to be powered through a single pressure source such as an electromechanical pump, in a *direct actuation* paradigm, each actuator would still require a dedicated electromechanical valve for independent operation. Thus, a practical challenge in designing soft robots with many degrees of freedom (DOF) is the size, cost, and modularity of common electromechanical components (e.g., solenoid valves, pumps, relays, etc.),^[4,9,14] which in a direct actuation paradigm scale linearly with the number of DOF (**Figure 1**). Efforts to miniaturize electromechanical valves and pumps have proven beneficial.^[15–18] However, miniaturization of valves and pumps decreases performance metrics such as control bandwidth, maximum pressure, and viscous losses.^[9] Alternatively, pumps actuated using electrostatic forces have been demonstrated for controlling each actuated DOF.^[19,20] However, these pumps are not capable of displacing large volumes and generating high flow rates as desired in many soft robotic devices. Thus, *direct actuation* of soft robots

S. Jadhav, P. E. Glick, M. Ishida, C. Chan, I. Adibnazari, N. Gravish, M. T. Tolley

Department of Mechanical and Aerospace Engineering
University of California San Diego
La Jolla, CA 92093, USA
E-mail: tolley@ucsd.edu

J. P. Schulze
Department of Computer Science and Engineering
University of California San Diego
La Jolla, CA 92093, USA

P. E. Glick
Jet Propulsion Laboratory
California Institute of Technology
4800 Oak Grove Drive, Pasadena, CA 91109, USA

 The ORCID identification number(s) for the author(s) of this article can be found under <https://doi.org/10.1002/aisy.202300011>.

© 2023 The Authors. Advanced Intelligent Systems published by Wiley-VCH GmbH. This is an open access article under the terms of the Creative Commons Attribution License, which permits use, distribution and reproduction in any medium, provided the original work is properly cited.

DOI: 10.1002/aisy.202300011

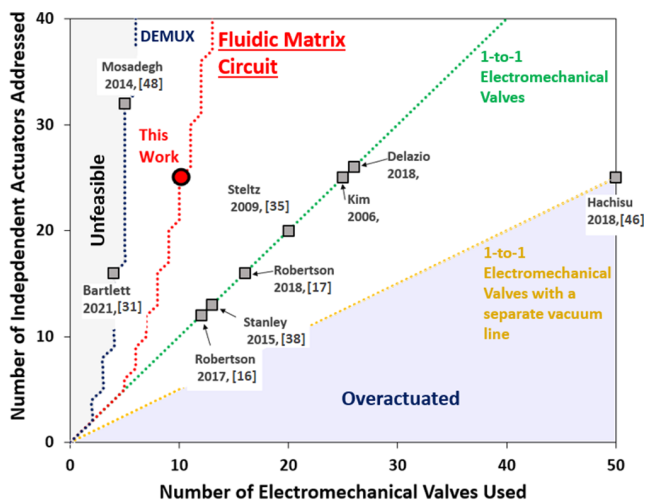


Figure 1. Comparison of the fluidic matrix circuit (FMC) with the conventional hardware used for fluidic control, including one-to-one electromechanical valves (*direct actuation*) and the fluidic demultiplexer presented in literature. The plot shows the number of individually addressable actuators controlled as a function of the number of electromechanical valves used in the system, as reported in previous literature. The FMC enables the control of 25 individually addressable actuators using only 10 electromechanical valves for input.

and haptic devices significantly restricts the maximum number of individually addressable DOF (Figure 1).

One attempt to resolve the design issues associated with electromechanical components is the development of electronics-free pneumatic controllers.^[21–25] For example, pneumatic circuits that rely on self-sustained pneumatic oscillators enable continuous periodic actuation of soft robots without electromechanical components have been presented recently.^[21–26] A common design paradigm for this is a soft, bistable valve that uses a pressure signal to switch the state of the internal membrane and to control the airflow.^[22] These valves can be combined to create more sophisticated control elements such as logic gates, shift registers, pressure sensors,^[21] and oscillating circuits inspired by central pattern generators (CPGs) in nature.^[23,27] Similar approaches for the design of fluidic circuits using equivalent fluidic circuit elements like transistors, diodes, and pressure-driven oscillators have been presented.^[28–30] For example, Gallardo et al. presented a soft fluidic amplifier that can be used as a component to construct fluidically driven computing circuits for autonomous soft robots.^[30] Alternatively, coordination of multiple DOF through viscous flow dynamics within the pneumatic circuit can produce rich and adaptive actuator behaviors.^[31,32] Similar approaches for periodic sequential flow generation have also been implemented in microfluidics^[33] However, these design approaches do not rely on valves for controlling each individual actuator and thus are capable of actuating many DOF through a common pressure source and without electromechanical components. Both of these design approaches are only capable of a limited number of actuation patterns,^[31,32] and the system cannot be reprogrammed during operation.^[4,9] Thus, the scalability and controllability of soft robots are still severely restricted when using current approaches that employ electronics-free pneumatic circuits.

A promising method for addressing the scalability of actuation for soft robots is inspired by electronic demultiplexer circuits.^[34,35] A fluidic demultiplexer is a pneumatic subsystem that uses combinations of multiple flow lines using valve valves to control individual actuators.^[36] Through appropriate design, these systems are capable of drastically reducing the required number of electromechanical valves (N) required to independently control a large array of actuators (2^{N-1} ; Figure 1A). Fluidic demultiplexers were initially developed based on micro-fluidic valves^[37] suitable for applications that had low flow rates.^[6] More recently, control of large array of soft actuators using time-division multiplexing has been demonstrated at larger scales for soft robotics applications.^[34,38] A major challenge of fluidic demultiplexers for robotics and haptics applications is that they are in general only able to control actuator at a time.^[34] Thus, the refresh interval of an actuator array increases proportionally with the number of actuators^[9,34] (Figure 7B). These limitations in the control bandwidth of individual actuators due to viscous effects lead to a high refresh time for an array of actuators and make this control method impractical for many applications that require high bandwidths and flow rates.

A fluidic demultiplexer circuit has been inspired from a electronic demultiplexer that is commonly used for applications such as to control 7-segment displays.^[39,40] However, large form-factor light-emitting diode (LED) displays (commonly known as *dot-matrix displays*) avoid using demultiplexing, but instead use a fundamentally different circuit design. A *dot-matrix displays* consists of LEDs arranged in a 2D matrix with cathodes connected together in each row and anodes connected together in each column^[39,40] (see supplemental section *Electrical Inspiration for the Fluidic Matrix Circuit: the Dot-Matrix Display* for more details). The circuit is then time multiplexed to display an image on the *dot-matrix display*. This approach design enables a compromise between the number of independent inputs needed to control large array of LEDs and the maximum refresh rate for the dot-matrix display. We analyzed this fundamental working principle of the dot-matrix display circuit used to control a large LED display (i.e., in a dot-matrix display)^[39,40] to conceive the design of our fluidic system (Figure S1, Supporting Information). The basic element in the display, an LED, is analogous to a resistor element with a p–n junction diode. However, an actuator (or a bladder) in a fluidic system is an equivalent to a capacitor and cannot represent a direct analog to an LED for the equivalent fluidic circuit. Hence, constructing a fluidic circuit equivalent to a dot-matrix display required an intermediate circuit element that can generate an actuation signal based on the state of the mass flow through the circuit element (**Figure 2B**). Based on these requirements, we designed a fluidic circuit consisting of “fluidic logic modules (FLMs)” as intermediate circuit elements in an array analogous to the dot-matrix display (Figure 2A–C). The FLM produced vacuum and positive pressure at the output line based on whether the mass flow through it is enabled or disabled (Figure 2D–F). These FLMs were connected within a matrix we called a “fluidic matrix circuit (FMC)” that enabled the individually addressing any actuator in a large array as shown in (Figure 2).

This work presents a fundamentally different approach to the independent control of many pneumatic actuators that bridges

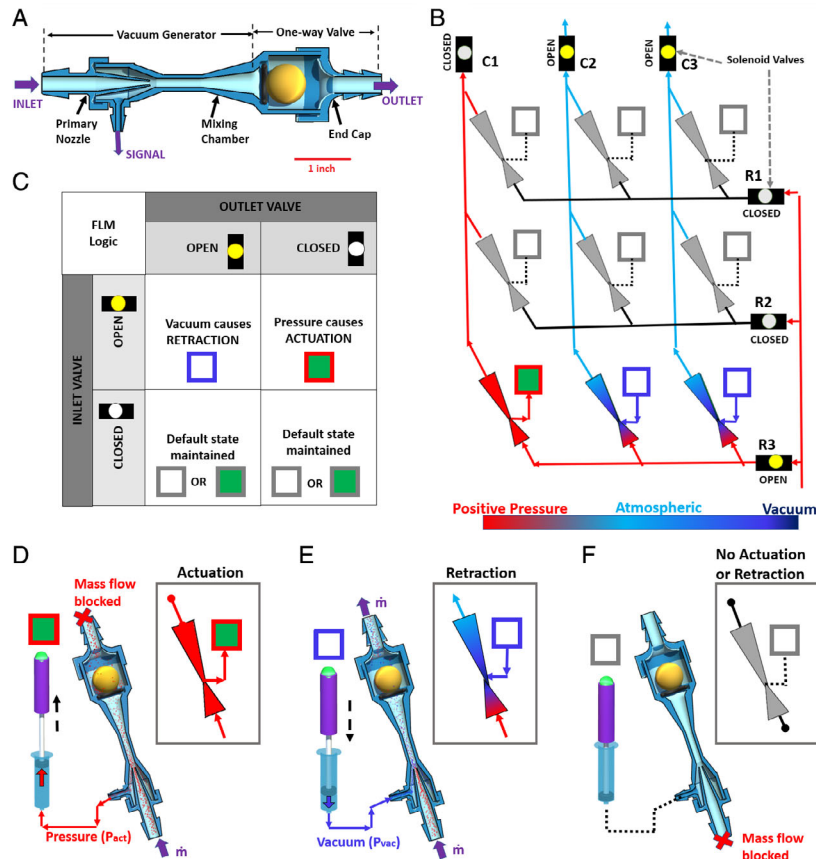


Figure 2. Design and construction of a fluidic matrix circuit (FMC) and a fluidic logic module (FLM). A) The fundamental unit of a FMC is a fluidic logic module (FLM) consisting of a vacuum generator connected in series to a custom-made one-way valve. The output pressure in the signal line of the FLM controls the actuator corresponding to the FLM. B) Schematic of a 3×3 FMC consisting of nine (9) FLMs connected in a matrix. Each FLM is connected to one actuator. The FMC is controlled by sequentially addressing each row within the matrix using six (6) electromechanical valves. C) Logic explaining how the switching of electromechanical valves is used to control the signal pressure from the FLM. D,E) When the pressure at the inlet of the FLM is enabled, the state of the mass flow at the outlet is used to modulate the signal in the output line between positive pressure and vacuum. F) When there is no pressure differential at the inlet of the FLM, the actuator retains its default state. Note that the boundary color of the actuator symbol indicates the internal pressure, while the inner color indicates the state of the actuator.

the tradeoffs between *direct actuation* and fluidic demultiplexing. Inspired by electronic circuits that drive dot-matrix display, we call this fluidic subsystem a *FMC* which enables the independent control of a large array of actuators while using a limited number of electromechanical valves (Figure 1). This work makes the following contributions to the field of fluidically actuated robotics: 1) efficient control technique for distributed DOF: we present a fluidic circuit matrix inspired by a dot matrix display to individually address a large array of actuators (N^2) using a limited number ($2N$) of electromechanical valves (Figure 2). Our proposed fluidic circuit has a potential to achieve a refresh rate that is an order of magnitude higher than demultiplexers previously presented in the literature (Figure 7B); 2) Versatility of control hardware: our control hardware is capable of generating both positive pressure and vacuum without using any external vacuum pumps, which is highly beneficial for many applications in soft robotics. We demonstrate the versatility of our control hardware by controlling a shape display composed of 5×5 tactors^[41] and a wearable haptic vest; and 3) mathematical

modeling using analogous electrical circuit: we present a lumped-parameter, dynamic response model for our fluidic circuit to understand the relationship between the key system parameters and the dynamic response of the circuit. Together, these contributions enable fluidic control hardware that has the potential to enable more complex and sophisticated soft robotic devices that have been envisioned in the literature.^[42–46]

2. Results

2.1. Design and Construction of the Fluidic Logic Module

An FLM consisted of a vacuum generator device (specifically, a double-stage Venturi) connected in series with a one-way valve (Figure 2A and S2, S3, Supporting Information). The vacuum generator consisted of three main sections—a primary nozzle, a mixing section, and a diffuser (Figure 2A and S2, S3, Supporting Information). When a pressure source was connected at the inlet of the vacuum generator, the primary nozzle

accelerated the airflow as described by Bernoulli's equation. This high velocity, low static pressure air flow exiting the primary nozzle induced a secondary flow from the suction chamber and accelerated it along with the mixing chamber (Figure 2A,E). This mass flow through the vacuum generator generated a vacuum at the signal line connected to the actuator (Figure 2E). When the mass flow through this vacuum generator was blocked at the outlet of the vacuum generator, the steady-state pressure in the signal line connected to the actuator was equal to the pressure at the inlet of the vacuum generator (i.e., downstream pressure, Figure 2D). When there was no pressure at the inlet of the FLM, the pressure in the signal line was atmospheric pressure (Figure 2F). Thus, we can generate a bidirectional (positive pressure/vacuum) pressure in the signal line based on the states of the electromechanical valve connected to the corresponding FLM.

Building on the vacuum generator designs reported in the literature,^[47–49] we conducted empirical tests to determine the design parameters of a vacuum generator used in the FLM. Since the design of an FMC was a system design and integration problem involving a complex network of fluidic resistances, optimizing the vacuum generator as a stand-alone component would not necessarily reflect an optimum system design when the vacuum generator was integrated with the full FMC (see supplementary section “*Design and fabrication of FMC*” and “*Effect of the system resistance on the performance of the FMC*” for more details). Since the cross-section at the exit of the primary nozzle was the narrowest constriction within the FLM, the diameter at the exit of the primary nozzle was the most significant factor that determined the fluidic resistance of the FLM^[50]. We considered the tradeoffs between the fluidic resistance of the vacuum generator and the maximum vacuum generated by the FLM and selected the vacuum generator with a 1.39 mm diameter at the exit of the primary nozzle as the optimum in our use case (see supplementary sections “*Effect of the system resistance on the performance of the FMC*” and “*Characterization of FLM*” for more details).

The one-way valve in the FLM prevented the backflow of air into the FLM and insulated the rows in the FMCs from any cross-interference from the pressure signal inside the columns. Without a one-way valve, the mass flow through an activated FLM generated an undesired pressure signal along the neighboring FLMs connected to the same column. The one-way valve design consisted of a glass marble that was loaded by gravity on an O-ring (Figure 2A).

2.2. Working Principle of the Fluidic Matrix Circuit

The working principle of the FMC was inspired by an equivalent electrical circuit found in an LED dot-matrix display.^[39,40] The FMC was a 2D matrix of FLMs where the inlets of all FLMs connected together for each row and outlets of all FLMs connected together for each column (Figure 2B). An actuator connected to any FLM within the matrix was individually addressed by controlling the mass flow through the two electromechanical valves connected to the corresponding row and column of that FLM within the matrix (Figure 2B,C and Movie S1, Supporting Information). Similar to the dot-matrix display,^[39,40] the entire set of actuators

connected to the FMC was addressed one single row at a time. Thus, the working principle of the FMC can be explained by understanding how a single row of FLMs within the matrix was used to update the state of actuators connected to that row.

The array of actuators connected to the FMC was refreshed by sequentially addressing each row within the matrix for a short period of time (Figure 2B). A row of FLMs connected to one inlet manifold within the FMC was addressed by opening the electro-mechanical valve at the inlet, enabling the airflow through that manifold. Then, specific FLMs within the row were addressed by switching the states of the electromechanical valves in the respective columns connected to the outlets of the FLM (Figure S4 and Movie S1, Supporting Information). Figure S4, Supporting Information shows how the state of actuators connected to a single row of FLMs within the FMC gets updated from State-i to State-iv. In the default state, there was no pressure signal differential from the output lines, and the actuator maintains its state (Figure S4(State-i), Supporting Information). When the mass flow through the inlet was enabled, the output lines either have a pressure or vacuum signal depending on the state of the electromechanical valves on the output manifolds connected to the respective FLMs (Figure S4(State-ii), Supporting Information). The tactor (piston) was either extended (actuated) or retracted depending on the pressure signal from the FLM connected to the actuator (Figure S4(State-ii), Supporting Information). The pressure signal from the FLMs was switched by switching the states of the electromechanical valves on the output manifolds (columns in the FMC) for the corresponding FLM (Figure S4(State-iii), Supporting Information). This ability to control the pressure signal in the signal line for each FLM in the row enabled us to control the actuators connected to the FLMs (Figure S4(State-iv), Supporting Information). We created the FMC by arranging multiple such rows of FLMs in an array, where any actuator connected to a particular FLM within the matrix was actuated by addressing the two electromechanical valves connected to the corresponding row and column. Using this sample principle, we describe the implementation of the FMC to control a 2.5D-shape display and a haptic vest (Figure 4 and 6).

2.3. Analytical Model for the Fluidic Matrix Circuit

Since we operated the FMC by sequentially addressing each row of the matrix, we used pneumatic-electrical analogs to model an individual row of the FMC to understand the dynamics of the fluidic circuit (Figure 3C,D). Each individual row of the FMC was formed by connecting together multiple FLMs in parallel using an inlet manifold. The flow of air through this inlet manifold was controlled using a solenoid valve connected to a pressure source (Figure 3B). Since the diameter at the throat of vacuum generators within the FLMs (diameter at throat = 1.39 mm) was significantly smaller than the inner diameter of the inlet and outlet manifolds (inner diameter of the inlet manifold = 9.52 mm), the fluidic resistance of the manifold was neglected. Hence, an individual row of the FMC can be represented as a lumped parameter system with FLMs represented as resistors R_v ^[50] (Figure 3C,D)). The resistance due to the bends in inlet manifold, solenoid valve, and the pneumatic connections between the pressure source and the input to the solenoid valve was

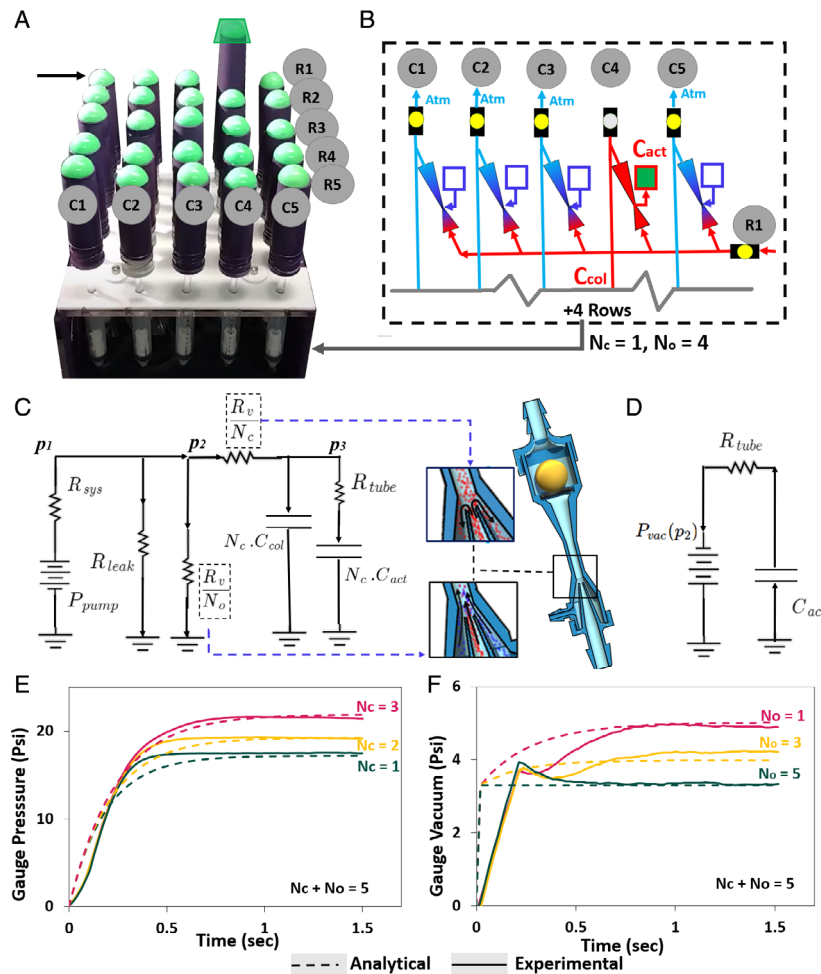


Figure 3. Design and modeling of the fluidic matrix circuit (FMC) connected to control a 5×5 shape display. The shape display A,B) containing 25 individually addressable actuators is controlled using a 5×5 fluidic matrix circuit (B). C,D) An equivalent electrical circuit (for actuation and retraction) for a single row of the FMC controlling the corresponding actuators on the 2D shape display. The FLM module can be represented as an equivalent fluidic resistance. The throat section within the primary nozzle of the FLM contributes majorly to the resultant fluidic resistance of the FLM. E,F) Representative trials showing the dynamic pressure response in the signal line controlling the actuators using the FMC during actuation (positive pressure, (E)) and retraction (vacuum, (F)). We used a source pressure of 30 psi, and R_{sys} was significantly higher as compared to other resistances (negligible leakage).

represented as R_{sys} . We used a single row (channel) of FMC (containing 5 FLMs) with an equivalent volume of outlet manifolds and actuators attached to each channel to measure the pressure response of the at each FLM. However, during operation of an integrated 5×5 FMC, an intentional leakage had to be introduced within inlet manifold of the FMC to avoid any pressure buildup within inlet manifolds due to leakage in the one-way valves. We used experimental methods to calculate the fluidic resistances within our FMC as $R_v = 12.979 \times 10^7$ and $R_{sys} = 2.4 \times 10^7 \text{ Pa}\cdot\text{s kg}^{-1}$ (see Supplemental sections “Characterization of the Fluidic Logic Module” and “Effect of the Resistance of the FLM on the System Performance” for more details).

The equivalent circuit parameters to predict the positive pressure response at the input to the actuators depending on the states of electromechanical valves connected to each column along the output manifolds. When the solenoid valve along the output manifold was closed, the air had to fill the entire

volume within the output manifold in addition to the volume of the actuator to generate a positive pressure response within the actuator (Figure 3C). This volume within the output manifold and the actuator was represented as an equivalent pneumatic capacitance C_{col} and C_{sys} , respectively^[50] (Figure 3C). This equivalent pneumatic capacitance was proportional to their respective internal volumes and calculated assuming isothermal compression, using Equation (1),^[50] where m is the mass of air within the capacitor, P is the pressure in the capacitor, M is the molecular weight of air, $T_{atm} = 298\text{K}$ is the atmospheric temperature, $R = 287 \text{ J kg}^{-1} \text{ K}^{-1}$ is the ideal gas constant

$$C_{res} = \frac{dm}{dP} = \frac{V_0 M}{RT} \quad (1)$$

The resistance of the tubing that connects the FLM to the actuator was modeled using the Darcy–Weisbach Equation (2),

where \dot{m} is the mass flow rate of air for a pressure drop of P along with the tubing, L is the length of the tubing, D is the diameter of the tubing, and μ is the viscosity of air. This tubing resistance was inversely proportional to the fourth power of the diameter of the tubing and could significantly affect the dynamic pressure response within the actuator when long and small diameter tubing (i.e., tubing with high resistance) was used to connect FMC with the individually addressable actuators

$$R_{\text{tube}} = \frac{\Delta P}{\dot{m}} = \frac{128\mu L}{\pi\rho D^4} \quad (2)$$

When the solenoid valve connected to a particular output manifold along the column was in a closed state, the steady-state pressure at the signal line from the FLM was equal to the downstream pressure in the input manifold (Figure 2B). The dynamic pressure response within the actuator connected to the signal line was modeled using the equivalent electrical circuit described in Figure 3C). The response time of the pressure within the actuator depended on the total number of solenoid valves in the open (N_{open}) and closed state (N_{closed}) ($N_{\text{closed}} + N_{\text{open}} = 5$). The circuit shown in (Figure 3C) is a second-order system, and the transfer function for the pressure response within the actuator was derived using Kirchoff's law. The transfer function for the pressure response during actuation is represented in Equation (3), where P , Q , and R are system parameters which are functions of N_{open} , N_{closed} , C_{col} , C_{col} , R_v , R_{sys} , and R_{tubing} (see supplemental section "Deriving the Dynamic Pressure Response of the F.M.C." for more details). Figure 2E shows the positive pressure response in the signal line with different combinations electromechanical valves in closed state

$$\frac{P_{\text{actuation}}(s)}{P_{\text{pump}}} = \frac{1}{Ps^2 + Qs + R} \quad (3)$$

When the solenoid valve connected to a particular output manifold along the column was in an open state, a steady-state vacuum was generated at the signal line of the FLM. The magnitude of the vacuum generated (P_{vac}) was a function of the pressure at the inlet of the FLM module (P_1). Figure 3D shows the circuit during retraction of the actuator when a vacuum was generated at the signal line of the FLM due to the entrainment effect in the vacuum generator. Figure 2F shows the vacuum response in the signal line with different combinations of electromechanical valves in closed state.

The dynamic pressure response calculated using the analytical model for a single row of the FMC can be used to predict the actuation period for each row and the refresh rate for the entire array of actuators controlled by the FMC. Figure 3E,F shows the representative trials for the pressure and vacuum response of a single row within the FMC. For our design, the steady-state pressure reduced with the increase in the number of valves in the open state (Figure 3E), and the steady-state vacuum increased with the decrease in the number of valves in open state ($N_{\text{closed}} = 0$ and $N_{\text{open}} = 5$) (Figure 3F). For the source (pump) pressure of 30 Psi, the (measured) maximum actuation pressure (in closed channels N_c) is 30 Psi when all the valves on the outlet channels (columns) are in closed state ($N_c = 5$, $N_o = 0$). The (measured) maximum vacuum pressure for the source pressure

of 30 Psi is 5.02 Psi when one valve connected to the outlet channel is having a solenoid valve in open state as shown in Figure 3F ($N_c = 4$, $N_o = 1$).

The reliability of the output parameters (time constant (τ_{act}), steady-state pressure (P_{act}), and vacuum (P_{vac})) for pressure response of the FMC calculated using the analytical model depends on the accuracy of the measured input parameters for the circuit (fluidic resistances (R_{sys} , R_v) and capacitance (C_{act} , C_{col})). We used Monte-Carlo simulation to analyze the effect of variability of design parameters of the circuit on the characteristic output for dynamic pressure response. The simulation shows a maximum error of $\pm 8.00\%$ (1.31 Psi) in the steady state pressure from the mean value (16.4 Psi), with 68% confidence in case of $N_c = 1$ ($N_o = 4$) (see Supplemental Section *Modeling the dynamic pressure response of FMC* for more details). Similarly, in case of the signal vacuum, the simulation shows a maximum error of $\pm 13.5\%$ (0.669 Psi) from the mean value (4.94 Psi vacuum), with 68% confidence in case of $N_c = 4$ ($N_o = 1$). The dynamic response of the FMC is absolutely stable, and any leakages within the system can be identified using the method described in *Modeling the Dynamic Pressure Response of FMC*.

2.4. Demonstrations Using the Fluidic Matrix Circuit

2.4.1. Shape Changing Display as a Pattern Generator

We demonstrated the implementation of our FMC for controlling a fluidically driven, shape-changing display with 25 independent actuators arranged in a 5×5 array (Movie S2 and S3, Supporting Information). Each actuator within the matrix consisted of a single-acting cylinder with a tactor (i.e., a probe) attached to the rod side of the piston. When the row corresponding to an actuator was addressed, the piston was either extended or retracted depending on whether there was positive pressure or vacuum signal from the FLM (Figure 2B,C). This two-dimensional array of actuators was refreshed by sequentially addressing each individual row within the matrix for a short period of time. The total refresh interval of the 2D-shape display was equal to the sum of the refresh intervals required to update the states of all actuators connected to each row (refresh interval for each row = 1.5 s). This 5×5 shape-changing display could be used as a tactile device to physically display information through static shape patterns (Figure 4 and Movie S2, Supporting Information). The shape-changing display could render various shape patterns including a variety of geometric patterns, numbers, letters, graphics, or incoming visual data from other devices (Figure 4 and Movie S2, Supporting Information). Figure 4 illustrates some examples to demonstrate the possible applications of our shape-changing display. Each frame of the information rendered on the 5×5 shape display was dynamically updated by sequentially addressing one row of tactors at a time (Figure 4A). In addition, we demonstrated the shape-changing display rendering every frame of a "Snake game", as the position of the "snake" was dynamically updated on a 5×5 grid (Figure 4B and Movie S3, Supporting Information).

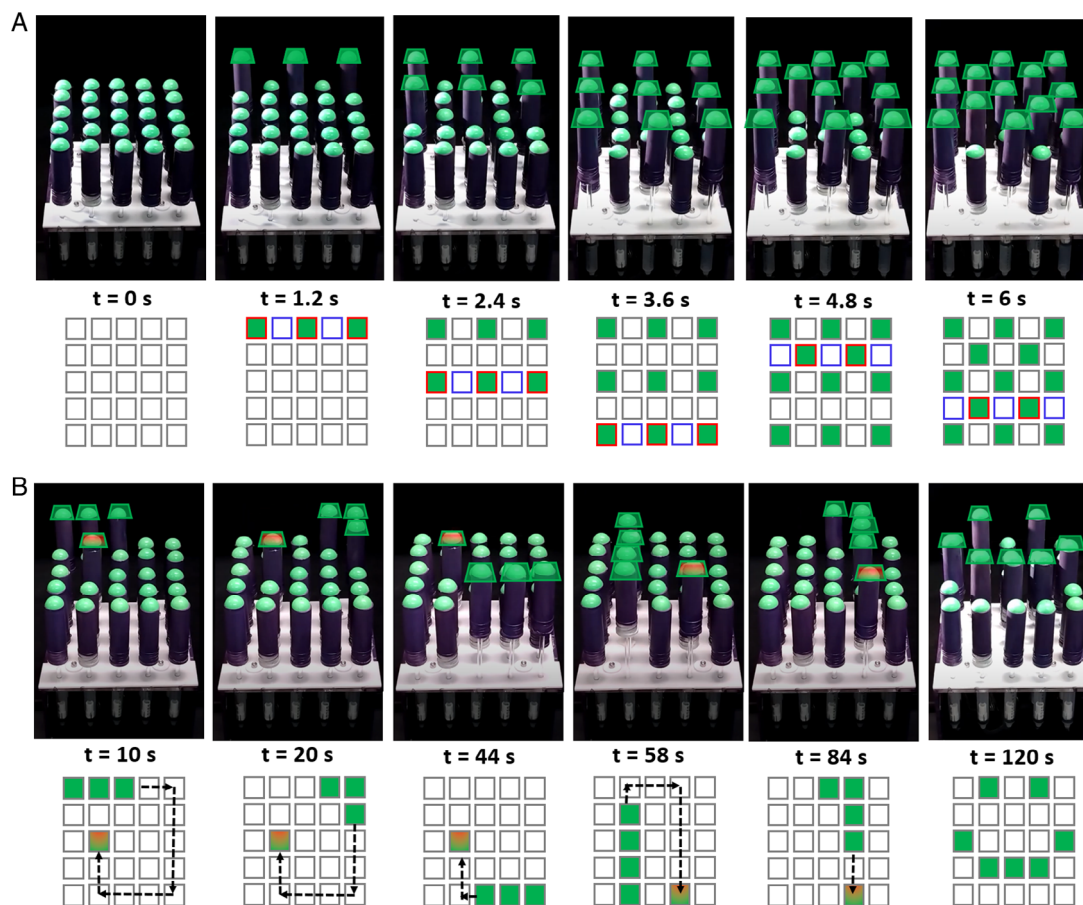


Figure 4. The fluidically driven, shape-changing display controlled using the FMC can render a variety of geometric data, graphics, and static patterns. The information rendered by these patterns can be perceived either visually or by moving the fingers over the display. A) Snapshots while sequentially updating the states of actuators in each row to display a checkerboard pattern. B) Snapshots of various frames that were rendered while simulating a “snake game” on a 5×5 grid. The shape display rendered a smile when the player wins.

Previous work had demonstrated a 5×5 interactive shape display controlled using a pneumatic system.^[51] Since the actuators in this display required both pressure and vacuum for operation, the pneumatic system to control such a 5×5 display consisted of 50 electromechanical valves (25 for pressure circuit and 25 for vacuum circuit) to be able to individually address each actuator. Our FMC was able to control a similar size (5×5) array, with similar actuation requirements, using ten (10) electromechanical valves.

2.4.2. Surface Profile Generator for Object Manipulation

We demonstrated the use of the 5×5 shape display, controlled by the FMC, to generate desired patterns to convey and manipulate objects (Figure 5 and Movie S4, Supporting Information). Tactors were used to generate height profiles to confine the object within a cage and to guide the motion of the object alongside the desired path (Movie S4, Supporting Information). As the rendered pattern changed, we leveraged the force generated by the dynamic actuation and retraction of tactors to move the object along the desired path (Figure 5). The height profile generated by

the shape display was also used as a passive constraint to arrest the motion of the objects during manipulation. We demonstrated the pattern generation for object manipulation to convey a ball along the row, column, and diagonal of the shape display (Figure 5 and Movie S4, Supporting Information). The ball weighed 141.5 g, and the average velocity of the ball was 0.2 m min^{-1} .

2.4.3. Pneumatically Powered Haptic Vest

We demonstrated the implementation of the FMC for controlling a haptic vest consisting of inflatable airbags that provided force feedback to the user when a bag was inflated (Figure 6 and Movie S5, Supporting Information). The haptic vest designs with inflatable airbags (pouch motors) with individually addressable electromechanical valves was inspired from.^[52] We designed a computer interface where the user clicked a button to actuate a corresponding pouch on the vest and experienced the sensation of being hit by a soft object (e.g., snowball) (Figure 6A and Movie S5, Supporting Information). When the user selected a pouch from the interface, the valve activated the corresponding row

An object transported across the surface with dynamic shape patterns

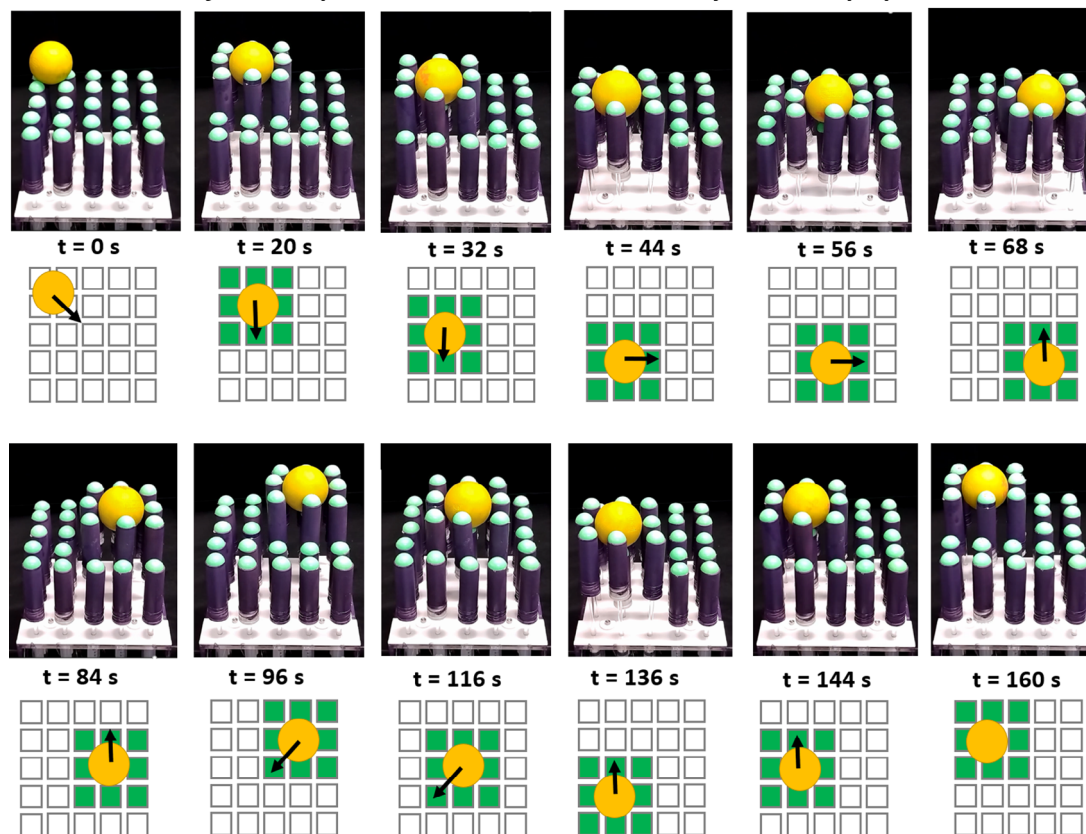


Figure 5. Demonstration of the shape display as a surface profile generator for object manipulation that is controlled using the FMC. Time lapse of 2D-shape display controlling and manipulating a spherical object. The height profile generated by the shape display is also used as passive constraints, and the object is manipulated in the desired direction by controlling the surface profile.

and column for the FLM connected to the pouch, which then inflated the pouch for 0.5 s (Figure 6A). The pouch was then rapidly deflated to give a sensation of being hit by a soft object. The deflation of the pouch was accelerated by generating a vacuum using the FLM corresponding to the pouch, rather than only relying on the elastic restoring force of the soft material. We calculated the response time (Figure 6B) of the pouches by using the equivalent electrical circuit previously described in Figure 3C,D. We compared the pressure response at the outlet connecting to the pouch with our analytical model (Figure 6B). We used a source pressure of 30 psi and measured the response without attaching the pouch to avoid any interference due to the dynamics of the pouch. The actuation pressure in the presence of the flexible pouch would be less than the measured value, and would depend on the fluidic capacitance and dynamics of the pouch. The discrepancy during vacuum can be attributed to the simplification in the analytical model which neglects the transition effects as the signal from the FLM instantaneously switched from positive pressure to vacuum.

3. Discussion

This work presented a novel fluidic control technique (using FMC) that addresses the challenge of controlling a large array

of individually addressable actuators using a limited number of electromechanical valves. Our approach was enabled by studying the fundamental working principle of a dot-matrix display circuit^[40] to conceive the components for an equivalent fluidic circuit. To test the concept of our equivalent fluidic circuit (viz. FMC), we prototyped a design of an FMC using an array of size 5×5 to control an array of 25 individually addressable actuators using only 10 electromechanical valves. We demonstrated the implementation of our control hardware to actuate a 5×5 shape display. We also demonstrated the implementation of FMC to control a wearable haptic vest for applications in virtual environments. We presented a lumped-parameter time response model to analyze the critical design parameters and predict the dynamic response of our system. The lumped-parameter circuit using equivalent electrical analogs was accurately able to predict the response times and the steady-state pressures within the circuit, and gives the general guidelines for how the changes in circuit parameters influence the performance of the system. The FMC was capable of achieving an actuation response of 2.2 Hz (or an actuation response time of 0.45 s). We believe that the FMCs are scalable and can control $N \times N$ actuators with $2N$ electromechanical valves with a refresh rate that is an order of magnitude higher than demultiplexing techniques presented in the previous work.^[34,35] In case of micro-fluidic demultiplexers, although a combination of demultiplexers can be used

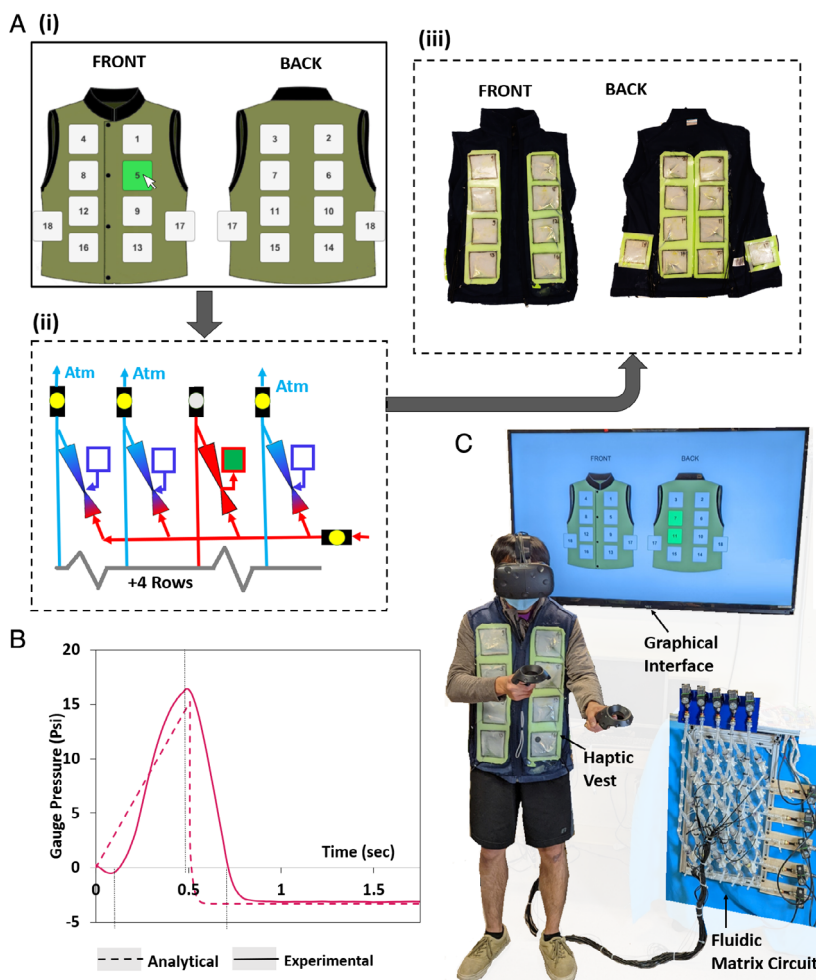


Figure 6. The fluidic matrix circuit (FMC) is used to control a pneumatically actuated haptic vest. A-i) A custom interface communicates with the electromechanical valves within the FMC A-ii) to activate the row and column corresponding to the FLM connecting to the pouch A-iii). The corresponding pouch A-iii, Figure S9, Supporting Information) on the haptic vest is inflated. B) Dynamic pressure response within the signal line in the absence of pouch (effectively a zero-volume pouch). The FMC pressurizes the pouch for 0.5 s and then vacuums it for evacuating the air inside. Actuation pressure is 30 psi. C) The user wearing the haptic vest for multimodal feedback while interacting with the VR environment. The front and back of the haptic vest was turned inside out to display the pouches on the vest. The haptic vest had 18 pouches connected to the fluidic circuit.

to decrease the total refresh interval (**Figure 7B**), they still do not offer the high refresh rates desired for many applications containing a large array of actuators. Additionally, our control approach using FMCs is versatile and can generate both positive pressure and vacuum, which is especially useful for applications in soft robotics.^[1,5,9] Since fluidic demultiplexing^[34,53] is the only other subsystem that allows for independent control of a large array of individually addressable actuators, we offer a qualitative comparison of our approach with fluidic demultiplexing in **Figure 7A**.

The fluidic system to control and manage several individually addressable actuators, as demonstrated in this work, has the potential to enhance the sophistication and complexity of many soft robotic devices reported in the literature, for e.g., refs. [42-44,46,54,55]. Several concepts of soft robotic devices presented in the literature have envisioned complex robot designs with many distributed DOF.^[3-5,9,55] However, due to limitations in the

control hardware, most of these envisioned concepts have been demonstrated with only a low-fidelity prototype.^[4,9] Many soft robotic devices described in the literature require the control hardware capable of managing several DOFs to achieve the potential that is envisioned, e.g., refs. [15,42-44,46,54]. The fluidic control hardware presented in this paper would enable the design of soft robotic devices with many distributed DOF that can be individually addressed. Additionally, the ability of an FMC to generate both positive pressures and vacuum is especially useful for controlling soft robots that simultaneously desire both vacuum and positive pressure for efficient fluidic actuation.^[5,51,52] This work also demonstrates the largest number of degrees-of-freedom controlled independently (25) with high flow rates, as compared to previous techniques used in soft robots.^[9]

The ability to independently control several actuators with minimal latency is of great interest for applications in haptic

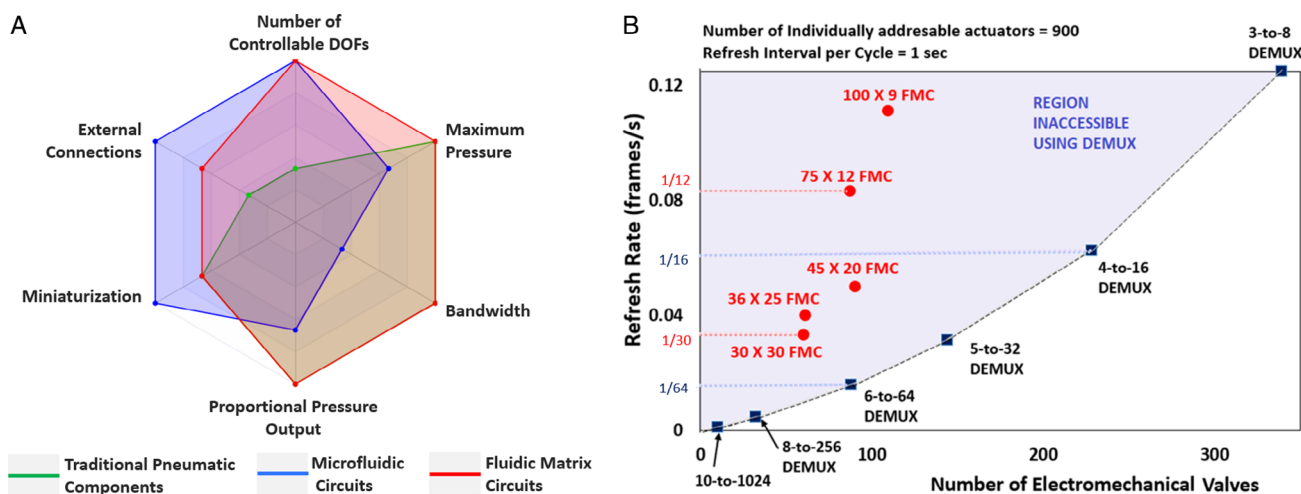


Figure 7. Qualitative comparison of the fluidic matrix circuit (FMC) with the conventional hardware used for fluidic control, including one-to-one electromechanical valves (traditional pneumatic components) and the fluidic demultiplexer (micro-fluidic circuits). A) Qualitative comparison of performance of FMC using criterias defined by McDonald et al.^[9] B) Theoretical approximations of refresh rates for 900 individually addressable actuators as a function of the number of electromechanical valves (using DEMUX and FMC). We assume the refresh interval per inflation cycle for an actuator as 1 s. The FMC enables controlling an individually addressable array of actuators with a refresh rate that is an order of magnitude higher as compared to using any combination of demultiplexer(s) using the same number of electromechanical valves. Refer Table S1, Supporting Information for more details on the calculation of the refresh rates.

displays.^[4] Previous work has demonstrated tactile displays and interfaces using fluidic systems for controlling the array of actuators on the display.^[4,46,56,57] However, similar to soft robotic devices, the number of individually addressable control lines available to address each actuator has restricted the resolution of these displays.^[45,46] Recently, commercial entities have developed a significant interest in designing fluidic logic circuits for reducing the number of electromechanical valves required to control a large array of actuators, especially for applications in wearable tactile gloves.^[58,59] The fluidic control methodology presented in this paper has a promise to make such tactile displays scalable by enabling a high resolution of actuator arrays that can be controlled without proportionally increasing the size or the cost of the control hardware.

This work presented here focused on a fundamental innovation in the system-level integration of fluidic systems by designing a fluidic circuit (FMC) inspired from an equivalent electrical analog (dot-matrix display). However, the design of the FMC presented in this paper requires steps for component and circuit assembly. In the future, we envision that such a circuit could be manufactured on a single chip using low-cost manufacturing techniques, like injection molding, which would make the sub-system compact. The current design of 5×5 FMC occupies a volume of $24 \times 14 \times 3$ cubic inches. However, we believe that the form factor of FMCs can be miniaturized using the designs of venturi tubes and check valves (basic components of FLM) reported in microfluidics.^[60,61] Although the demonstrations described in this paper have concentrated on controlling actuators that can hold their state, our fluidic system technique can also be used to control soft actuators if we introduce damping in the fluidic circuit. The modeling of the fluidic circuit presented in this paper might offer some insight into the methods by which damping can be introduced in the circuit; however, we

leave the detailed analysis for future work. The scalable FMC presented in this paper have the potential to enhance the complexity of fluidic devices used for applications in soft robotics and haptic interfaces.

4. Experimental Section

Design and Fabrication of the Fluidic Logic Module: The design of the FLM consisted of a vacuum generator in series with a one-way valve (Figure 2 and 3). The FLM consisted of three parts—the primary nozzle, the mixing chamber, and the end cap. All the parts were 3D printed using a commercial SLA printer (Form2, Formlabs Inc with ClearV4 resin). A neoprene O-ring with 1/2 inch inner diameter (I.D.) and 5/8 inch outer diameter (O.D.) is used at the interface between the primary nozzle and mixing chamber. A neoprene O-ring with 13/16 inch I.D. and 1 inch O.D. is used at the interface between the mixing chamber and end cap. These O-rings result in an air-tight assembly of the FLM. An end cap that can be detached facilitates the assembly of the one-way valve. The one-way valve consisted of a glass marble with an approximate diameter of 16.5 mm resting on a neoprene O-ring with 1/2 inch I.D. and 11/16 inch O.D. (see supplementary materials, “Design and Fabrication of Fluidic Logic Module” section for more details).

Assembly of the Fluidic Matrix Circuit: The FMC presented in this paper consists of 25 FLMs connected in an array of size 5×5 (5 rows and 5 columns) controlled using 10 direction control valves (Figure S3, Supporting Information). The FLMs are mounted on a wall-mounted acrylic sheet (with 60 mm horizontal spacing and 150 mm vertical spacing). The FLMs are secured using 3D-printed mounts and zip-ties.

The inlets to all (5) FLMs in a row are connected together using an inlet manifold. A 2/2 direction control (D.C.) valve (DVP2D series, Nitra pneumatics) connects the inlet manifold for each row to a pressure source. The outlets to all (5) FLMs in a column are connected together using an outlet manifold (Figure S3, Supporting Information). A 2/2 D.C. (DVP2D series, Nitra pneumatics) valve exhausts the outlet manifold to the atmosphere (Figure S3, Supporting Information). A soft plastic tubing with I.D. 3/8 inch and O.D. 1/2 inch was majorly used to connect all the fluidic

components (manifolds, FLMs, 2/2 valves) in a matrix circuit. The 2/2 D.C. valves were controlled using a microcontroller (Arduino Mega), using relays to step up the voltage to 24 V. The inlet and outlet manifolds were custom designed to avoid any sudden change in the direction of flow and to minimize the fluidic resistance.

Characterization of the Components Used in the Fluidic Matrix Circuit: We experimentally calculated the fluidic resistances for the fluidic logic module (R_v) and the fluidic control system ($R_{(sys)}$) within our operating pressure range (See Supporting Information, “Characterization of FLM” and “Effect of the system resistance on the performance of the FMC” sections for more details). We compared our experimental calculations for fluidic resistance with empirical results based on previous work. The transfer function for the dynamic response of the circuit was derived using Kirchoff’s law (see supplementary materials, “Transfer Functions to Calculate the Dynamic Pressure Response of the F.M.C.” section for more details).

Design and Fabrication of the Shape Display: The shape display consisted of a 2D array of actuators arranged in a 5×5 pattern (Figure S12, Supporting Information). Each actuator consisted of a syringe with a 16.5 mm diameter and 10 mL actuation volume. The actuators were mounted on a laser-cut section and each actuator was separated by 40 mm between them (Figure S12, Supporting Information). The piston side of the syringe was connected to a cylinder of diameter 25 mm, height of 100 mm, and weight of approximately 40 g. The stroke length of each actuator within the shape display is 55 mm (Figure S12, Supporting Information).

Design and Fabrication of the Pneumatically Actuated Haptic Vest: The haptic vest consisted of an array of 18 PET pouches embedded in a layer of silicone. These pouches were then attached to a medium-size vest to enable haptic feedback to the user on their upper body (Figure S11, Supporting Information). Each pouch was 60×60 mm, embedded in silicone (90×90), and separated by 120 mm from the adjacent pouches. The pouches were connected to the FMC with a tube with a length of 2.75 m and I.D. of 1/16 inch.

Supporting Information

Supporting Information is available from the Wiley Online Library or from the author.

Acknowledgements

We would like to thank Y.-L.P. for his in-depth discussions and suggestions during the conceptualization stage of the FMC. We would also like to thank S.C. for his insightful discussions and for his help with recording the demonstrations for the shape display. This work was supported by the Office of Naval Research (grant no. N00014-20-1-2373). The contribution of Paul Glick was supported by the NSTRF program and performed as part of the JPL Research Fellowship program at the Jet Propulsion Laboratory, California Institute of Technology, under a contract with the National Aeronautics and Space administration. M.I. is supported by National Defense Science and Engineering Graduate (NDSEG) Fellowship. Any opinions or findings expressed in this paper are those of the authors and do not reflect the views of funding agencies.

Conflict of Interest

The authors declare no conflict of interest.

Data Availability Statement

The data that support the findings of this study are available in the Supporting Information of this article.

Keywords

distributed control, electro-pneumatics, fluidic circuits, fluidic demultiplexing, fluidic Logic, shape display, soft Robots

Received: January 6, 2023

Revised: April 11, 2023

Published online:

- [1] C. Majidi, *Soft Rob.* **2014**, *1*, 5.
- [2] D. Rus, M. T. Tolley, *Nature* **2015**, *521*, 467.
- [3] H. Lipson, *Soft Rob.* **2014**, *1*, 21.
- [4] H. Bai, S. Li, R. F. Shepherd, *Adv. Funct. Mater.* **2021**, *31*, 2009364.
- [5] C. Laschi, B. Mazzolai, M. Cianchetti, *Sci. Rob.* **2016**, *1*, aah3690.
- [6] R. Z. Gao, C. L. Ren, *Biomicrofluidics* **2021**, *15*, 011302.
- [7] F. Ilievski, A. D. Mazzeo, R. F. Shepherd, X. Chen, G. M. Whitesides, *Angew. Chem.* **2011**, *123*, 1930.
- [8] M. Wehner, M. T. Tolley, Y. Mengüç, Y.-L. Park, A. Mozeika, Y. Ding, C. Onal, R. F. Shepherd, G. M. Whitesides, R. J. Wood, *Soft Rob.* **2014**, *1*, 263.
- [9] K. McDonald, T. Ranzani, *Front. Rob. AI* **2021**, *8*, 266.
- [10] P. Polygerinos, N. Correll, S. A. Morin, B. Mosadegh, C. D. Onal, K. Petersen, M. Cianchetti, M. T. Tolley, R. F. Shepherd, *Adv. Eng. Mater.* **2017**, *19*, 1700016.
- [11] E. Brown, N. Rodenberg, J. Amend, A. Mozeika, E. Steltz, M. R. Zakin, H. Lipson, H. M. Jaeger, *Proc. Natl. Acad. Sci.* **2010**, *107*, 18809.
- [12] S. Jadhav, M. R. A. Majit, B. Shih, J. P. Schulze, M. T. Tolley, *Soft Rob.* **2021**, *9*, 173.
- [13] J. Ou, L. Yao, D. Tauber, J. Steimle, R. Niiyama, H. Ishii, in *Proc. of the 8th Int. Conf. on Tangible, Embedded and Embodied Interaction*, Munich, Germany, February 16, **2014**, pp. 65–72.
- [14] C. D. Onal, in *Micro-and Nanotechnology Sensors, Systems, and Applications VIII*, Vol. 9836, International Society for Optics and Photonics, Baltimore, MD, May 25, **2016**, p. 983627.
- [15] M. A. Robertson, J. Paik, *Sci. Rob.* **2017**, *2*, aan6357.
- [16] M. A. Robertson, M. Murakami, W. Felt, J. Paik, *IEEE/ASME Trans. Mechatron.* **2018**, *24*, 16.
- [17] A. V. Prituja, H. Ren, in *2017 IEEE Int. Conf. on Real-time Computing and Robotics (RCAR)*, IEEE, Okinawa, Japan, July 14, **2017**, pp. 421–426.
- [18] A. Shtarbanov, in *Extended Abstracts of the 2021 CHI Conf. on Human Factors in Computing Systems*, Yokohama, Japan, May 8, **2021**, pp. 1–6.
- [19] R. Diteesawat, T. Helps, M. Taghavi, J. Rossiter, *Sci. Rob.* **2021**, *6*, abc3721.
- [20] P. Linnebach, G. Rizzello, S. Seelecke, *Smart Mater. Struct.* **2020**, *29*, 075021.
- [21] D. J. Preston, P. Rothemund, H. J. Jiang, M. P. Nemitz, J. Rawson, Z. Suo, G. M. Whitesides, *Proc. Natl. Acad. Sci.* **2019**, *116*, 7750.
- [22] P. Rothemund, A. Ainla, L. Belding, D. J. Preston, S. Kurihara, Z. Suo, G. M. Whitesides, *Sci. Rob.* **2018**, *3*, aar7986.
- [23] D. Drotman, S. Jadhav, D. Sharp, C. Chan, M. T. Tolley, *Sci. Rob.* **2021**, *6*, 51.
- [24] W.-K. Lee, D. J. Preston, M. P. Nemitz, A. Nagarkar, A. K. MacKeith, B. Gorissen, N. Vasios, V. Sanchez, K. Bertoldi, L. Mahadevan, G. M. Whitesides, *Sci. Rob.* **2022**, *7*, abg5812.
- [25] A. Nagarkar, W.-K. Lee, D. J. Preston, M. P. Nemitz, N.-N. Deng, G. M. Whitesides, L. Mahadevan, *Proc. Natl. Acad. Sci.* **2021**, *118*, 8.
- [26] L. Jin, A. E. Forte, K. Bertoldi, *Adv. Sci.* **2021**, *8*, 2101941.
- [27] D. J. Preston, H. J. Jiang, V. Sanchez, P. Rothemund, J. Rawson, M. P. Nemitz, W.-K. Lee, Z. Suo, C. J. Walsh, G. M. Whitesides, *Sci. Rob.* **2019**, *4*, 31.

- [28] S. Song, S. Joshi, J. Paik, *Adv. Sci.* **2021**, *8*, 2100924.
- [29] J. D. Hubbard, R. Acevedo, K. M. Edwards, A. T. Alsharhan, Z. Wen, J. Landry, K. Wang, S. Schaffer, R. D. Sochol, *Sci. Adv.* **2021**, *7*, abe5257.
- [30] E. Gallardo Hevia, C. M. McCann, M. Bell, N.-s. P. Hyun, C. Majidi, K. Bertoldi, R. J. Wood, *Adv. Intell. Syst.* **2022**, *4*, 2200122.
- [31] N. Vasios, A. J. Gross, S. Soifer, J. T. Overvelde, K. Bertoldi, *Soft Rob.* **2020**, *7*, 1.
- [32] C. C. Futran, S. Ceron, B. C. Mac Murray, R. F. Shepherd, K. H. Petersen, in *2018 IEEE Int. Conf. on Soft Robotics (RoboSoft)*, IEEE, Livorno, Italy, April 24, **2018**, pp. 473–478.
- [33] Z. Li, S.-J. Kim, *Sci. Adv.* **2019**, *5*, aat3080.
- [34] N. W. Bartlett, K. P. Becker, R. J. Wood, *Soft Matter* **2020**, *16*, 5871.
- [35] W. H. Grover, R. H. Ivester, E. C. Jensen, R. A. Mathies, *Lab Chip* **2006**, *6*, 623.
- [36] T. Thorsen, S. J. Maerkl, S. R. Quake, *Science* **2002**, *298*, 580.
- [37] M. A. Unger, H.-P. Chou, T. Thorsen, A. Scherer, S. R. Quake, *Science* **2000**, *288*, 113.
- [38] S. Hoang, K. Karydis, P. Brisk, W. H. Grover, *Plos One* **2021**, *16*, 0254524.
- [39] A. Sawhney, P. Sawhney, *A Course in Mechanical Measurements and Instrumentation*, Vol. 3, Dhanpat Rai, New Delhi, India **1995**.
- [40] J. A. Castellano, *Handbook of Display Technology*, Academic Press Inc (Elsevier) **1992**.
- [41] G. Moy, C. Wagner, R. S. Fearing, in *Proc. 2000 ICRA. Millennium Conf. IEEE Int. Conf. on Robotics and Automation. Symposia Proceedings (Cat. No. 0CH37065)*, Vol. 4, IEEE, San Francisco, CA, April 24, **2000**, pp. 3409–3415.
- [42] E. Steltz, A. Mozeika, N. Rodenberg, E. Brown, H. M. Jaeger, in *2009 IEEE/RSJ Int. Conf. on Intelligent Robots and Systems*, IEEE, St Louis, MO, October 11, **2009**, pp. 5672–5677.
- [43] A. A. Stanley, J. C. Gwilliam, A. M. Okamura, in *2013 World Haptics Conf. (WHC)*, IEEE, Daejeon, South Korea, April 14, **2013**, p. 25.
- [44] D. S. Shah, M. C. Yuen, L. G. Tilton, E. J. Yang, R. Kramer-Bottiglio, *IEEE Rob. Autom. Lett.* **2019**, *4*, 2204.
- [45] A. A. Stanley, A. M. Okamura, *IEEE Trans. Haptic.* **2015**, *8*, 20.
- [46] M. Koehler, N. S. Usevitch, A. M. Okamura, *IEEE Trans. Rob.* **2020**, *36*, 613.
- [47] C. Liao, *Gas Ejector Modeling for Design and Analysis*, Texas A&M University, College Station, TX **2008**.
- [48] G. Emanuel, *AIAA J.* **1976**, *14*, 1292.
- [49] J. H. Keenan, E. P. Neumann, F. Lustwerk, *J. Appl. Mech.* **1950**, *17*, 299.
- [50] A. A. Stanley, A. Amini, C. Glick, N. Usevitch, Y. Mengüç, S. J. Keller, *J. Dyn. Syst. Meas. Control* **2021**, *143*, 051001.
- [51] T. Hachisu, M. Fukumoto, *IEEE Comput. Graph. Appl.* **2018**, *38*, 54.
- [52] A. Delazio, K. Nakagaki, R. L. Klatzky, S. E. Hudson, J. F. Lehman, A. P. Sample, in *Proc. of the 2018 CHI Conf. on Human Factors in Computing Systems*, Montreal, Canada, April 21, **2018**, pp. 1–12.
- [53] B. Mosadegh, A. D. Mazzeo, R. F. Shepherd, S. A. Morin, U. Gupta, I. Z. Sani, D. Lai, S. Takayama, G. M. Whitesides, *Lab Chip* **2014**, *14*, 189.
- [54] K. P. Becker, Y. Chen, R. J. Wood, *Adv. Funct. Mater.* **2020**, *30*, 1908919.
- [55] H.-Y. Chen, R. S. Diteesawat, A. Haynes, A. J. Partridge, M. F. Simons, E. Werner, M. Garrad, J. Rossiter, A. T. Conn, *Front. Rob. AI* **2019**, *6*, 52.
- [56] A. A. Stanley, K. Hata, A. M. Okamura, in *2016 IEEE Int. Conf. on Robotics and Automation (ICRA)*, IEEE, Stockholm, Sweden, May 16, **2016**, p. 2718.
- [57] Y. Kim, I. Oakley, J. Ryu, in *2006 SICE-ICASE Int. Joint Conf.*, IEEE, Busan, South Korea, October 18, **2006**, pp. 1933–1938.
- [58] S. J. Keller, J. Lindsay, S. Turkyilmaz, J. M. Lutian, T. T. Trutna, A. A. Stanley, Facebook Technologies, LLC, Menlo Park, CA, USA Patent App. 17/523,484, **2022**.
- [59] J. Perret, E. Vander Poorten, in *ACTUATOR 2018; 16th Int. Conf. on New Actuators*, VDE, Bremen, Germany, June 25, **2018**, pp. 1–5.
- [60] J. Hyeon, H. So, *Biomed. Microdevices* **2019**, *21*, article no. 19.
- [61] H. Yu, D. Li, R. C. Roberts, K. Xu, N. C. Tien, *J. Micromech. Microeng.* **2012**, *22*, 035010.